Journal of Alloys and Compounds 750 (2018) 577–586

Contents lists available at ScienceDirect

Journal of Alloys and Compounds

journal homepage: http://www.elsevier.com/locate/jalcom

Investigation of the Fe-Mo electrodeposition from sorbitol alkaline bath and characterization of the films produced

Maria G. Zacarin [a], Matheus M. de Brito [a], Elton P. Barbano [a], Rose M. Carlos [a], Valmor R. Mastelaro [b], Ivani A. Carlos [a, *]

[a] Department of Chemistry, Federal University of São Carlos, CP 676, 13565-905, São Carlos, SP, Brazil
[b] Institute of Physics of São Carlos, University of São Paulo, C.P. 369, 13560-970 São Carlos, SP, Brazil

ARTICLE INFO

Article history:
Received 7 April 2017
Received in revised form
29 March 2018
Accepted 2 April 2018
Available online 5 April 2018

Keywords:
Iron-molybdenum alloy
Electrodeposition
Sorbitol alkaline bath
Molybdenum oxide
Induced deposition

ABSTRACT

The electrodeposition of Fe-Mo alloys from an alkaline solution containing sorbitol as the complexing agent for Fe(III) ions was studied. XRD analysis of the film produced by reduction of $[MoO_4]^{2-}$ anions at a copper substrate showed the formation of MoO_2. The presence of the intermediate Fe(II) species was detected by electrolysis from an Fe-Mo solution and Visible spectroscopy of the final solution in the presence of 1,10-phenanthroline. The Visible spectrum showed a broad absorption ($\lambda_{max} = 514$ nm) typical of the $[Fe(phen)_3]^{2+}$ complex. Under our conditions, the Fe-Mo alloy was formed from reduction of $[Fe(OH)_2(C_6H_{12}O_6)_2]^{3-}$ to $[Fe(OH)_2(C_6H_{12}O_6)_2]^{4-}$, reduction of $[MoO_4]^{2-}$ to molybdenum (IV) oxide/hydroxide and its further reduction to Mo^0 concomitant with $[Fe(OH)_2(C_6H_{12}O_6)_2]^{4-}{}_{ads}$ to Fe^0. Photomicrographs of the Fe-Mo electrodeposits produced with q_d 5.30Ccm^{-2} showed that they were smooth or contained cracks, depending on the deposition potential (E_d). Chemical composition analysis by EDXS of Fe-Mo electrodeposits (q_d 5.30Ccm^{-2}) showed that deposits containing 5.5 at% (18.8 wt%) Mo could be produced at E_d −1.40 V and similar values were obtained at more negative potentials. X-Ray diffraction indicated that the Fe-Mo coatings were composed of Fe_3Mo and Fe_2MoO_4 phases, regardless of E_d. The presence of the Fe_2MoO_4 phase on the sample surface could explain the observation of Fe^{2+} and Mo^{4+} states by XPS, although the occurrence of others crystalline oxide phases, such as $FeMoO_4$ and $Fe_2(MoO_4)_3$ could not be discarded. The crystal size value varied from ~47 nm to ~37 nm, when E_d changed to more negative values.

1. Introduction

Studies concerning the electrodeposition of molybdenum alloys have been receiving attention in recent years due to the relevant properties of these materials, such as, high hardness, thermal and corrosion resistance and special magnetic properties [1]. The Fe-Mo codeposition process is classified as induced codeposition [1]. This alloy can be formed from molybdenum oxide or hydroxide reduction to Mo^0 and in the presence of metal iron (Fe^0) [2–5]. The alkaline baths for Fe-Mo electrodeposition contain, in general, ammonia for keeping the pH of the solution at ~10.0 [2,3,6]; which volatilize representing a disadvantage.

In our laboratory we have investigated the use of polyalcohols (mannitol, sorbitol and glycerol), to improve the characteristics of electrodeposits and in the stabilization of deposition baths of Cu [7,8], Zn-Ni [9], Zn [10,11], Ni [12], Fe-Zn [13], Cu-Zn [14], Pb-Sn [15], and Cu-Sn [16].

Thus, the goal of this study was to examine the stages of Fe-Mo electrodeposition from an alkaline bath, which contained sorbitol as a complexing reagent of Fe(III) ions (pH adjusted with NaOH), and to propose a mechanism for the Fe-Mo electrodeposition.

2. Experimental details

The Fe-Mo, Fe and molybdenum oxide/hydroxide electrodepositions were investigated, respectively, from 0.100 M $FeCl_3.6H_2O$ + 0.070 M $Na_2MoO_4.2H_2O$ + 0.200 M sorbitol, 0.100 M $FeCl_3.6H_2O$ + 0.200 M sorbitol and 0.070 M Na_2MoO_4 + 0.200 M sorbitol baths. The pH of these solutions was adjusted to pH 11.40 with NaOH concentrated solution. This pH was used, since the potentiometric titration of Fe-Mo deposition bath, containing 0.100 M $FeCl_3$ +

* Corresponding author.
E-mail address: diac@ufscar.br (I.A. Carlos).

https://doi.org/10.1016/j.jallcom.2018.04.020
0925-8388/

0.070 M Na_2MoO_4 + 0.200 M sorbitol, against 0.9558 M NaOH solution showed that at pH below 11.40 this bath presented precipitated of [Fe(OH) ($C_6H_{12}O_6$)] [17]. Therefore, the pH 11.40 was chosen to prepare the solutions reported previously. These solutions were prepared with reagents of analytical grade and with water distilled and deionized.

The working electrode was a Cu electrolytic disk (0.196 cm^2), which, immediately before the electrochemical experiments, was polished with 1200 emery paper, and then rinsed with water distilled and deionized and was quickly put in the electrochemical cell. The auxiliary (0.63 cm^2) and reference electrodes were respectively, a platinum plate, and a $Hg|Hg_2Cl_2|KCl$ (1.0 M), E = 0.268 V, with a Luggin capillary containing 1.0 M KCl solution. The cathode-to-anode area ratio was 0.31. The bath volume in the electrochemical cell was 50.0 mL.

The electrochemical measurements (voltammetric and potentiostatic electrodepositions) were performed using a microcomputer-controlled AUTOLAB potentiostat/galvanostat with PGSTAT 128 N equipment, processed by the GPES software. Cyclic voltammetry (CV) was used to investigate the deposition process. Hydrodynamic measurements were carried out with a Princeton Applied Research (PAR) ring-disk electrode system, model 636. The temperature was maintained at 25.0 °C.

The synthesis of $Na_3[Fe(OH)_2(C_6H_{12}O_6)_2]$ was performed as following: $FeCl_3.6H_2O$ (0.100 mol) was dissolved in H_2O (10.00 mL), and the sorbitol (0.200 mol) ligand was added; after this, 0.400 mol NaOH was added to this solution. The pH of the solution was 11.40. The solution was stirred after addition of each reagent. The final volume of the solution was 50.00 mL. Acetone was added in order to precipitate the complex. The dark red precipitate was left to decant and allowed to dry in a desiccator under vaccum.

C,H analysis was employed to characterize the Fe(III)-sorbitol complex present in the Fe-Mo bath, since the species present in the bath influence the electrodeposition process. The C,H elemental analysis for the Fe-sorbitol complex was performed using a Fisons EA 1108 CHNS-O equipment.

Chemical, morphological and structural characterization of Fe-Mo electrodeposits were produced at several deposition potential (E_d) with a deposition charge density (q_d) of 5.30Ccm^{-2}.

To investigate if the codeposition of Fe and Mo occurs from this bath and the influence of the electrodeposition potential on the morphology, composition and structure of the deposit, Scanning electron microscopy (SEM), Energy dispersive X-ray spectroscopy (EDXS) and X-ray diffraction (XRD) analyses of the Fe–Mo deposits were performed, respectively. SEM micrographs were taken using an Inspect S 50 electron microscope. Semi-quantitative chemical analysis of the electrodeposits by EDXS was carried out using an EDAX detector model Apollo. The accelerating voltage was 25 kV. The electrodeposits as prepared were removed from the electrochemical cell, rinsed with water distilled and deionized and quickly allowed to dry in a desiccator under vacuum until SEM, EDXS and XRD analyzes were performed. The structural phases of electrodeposits were investigated using a Rigaku Rotaflex RU200B X-ray generator equipped with a goniometer, in 2θscanning mode (from 2θ = 3.0° to 120.0°, in steps of 0.5°/min). The curved graphite monochromator was used to select the Cu Kα radiation (1.5406 Å). Also, the structural characterization was investigated by X-ray diffraction (XRD) using a Rigaku Ultima IV diffractometer using a grazing incidence geometry (θ = 1°) Cu-*Kα* (λ = 1.5418 Å) radiation and a LiF(100) monochromator. The XRD data were measured in a step-scan mode, in a range of 2θ = 30°–60° with a rate of 0.02°/5 s.

The chemical surface analysis of Fe-Mo electrodeposits was performed by X-ray photoelectron spectroscopy (XPS) using a conventional XPS spectrometer (Scienta Omicron ESCA+) with a high-performance hemispheric analyzer (EAC2000) with monochromatic Al Kα ($h\nu$ = 1486.6 eV) radiation as the excitation source. The operating pressure in the ultra-high vacuum chamber (UHV) during the analysis was 10^{-9} Pa. The XPS high-resolution spectra were recorded at constant pass energy of 20 eV with a 0.05 eV per step. The binding energies (BEs) were evaluated using C1s spectrum (BE = 284.6 eV) as the reference with a resolution of ±0.1 eV. The Ar ion bombardment of the Fe-Mo sample was performed in the XPS spectrometer. Before removing material from the sample, a high resolution spectra of C 1s, O 1s, Fe 2p and Mo 3 d elements were recorded from the surface of the sample. The surface was then etched by rastering an Ar ion beam over a quite rectangular area of the sample with an ion energy of 4.8 KeV and ion gun emission current of 13.5 mA. After the etch cycle, the ion beam was stopped and another set of high-resolution spectra was recorded. This sequence of etching and spectrum acquisition was repeated until 160 min of etching time.

Chemical analysis by Visible spectroscopy was performed to characterize the presence of the intermediate Fe(II) species. Visible spectra were recorded using an Agilent 8453 spectrophotometer.

3. Results and discussion

3.1. Characterization of $Na_3[Fe(OH)_2(C_6H_{12}O_6)_2]$

The complex was synthesized by the reaction of $FeCl_3.6H_2O$ with sorbitol in aqueous solution (pH 11.40).

The composition was evident from the C,H analysis: Anal. Calcd. for $Na_3[Fe(OH)_2(C_6H_{12}O_6)_2]$: C, 27.74%; H, 5.01%.

Found: C, 25.79%; H, 4.90%.

3.2. Fe-Mo voltammetric electrodeposition studies

Cyclic voltammetry was performed for the Cu substrate in the 0.100 M $FeCl_3$ + 0.070 M Na_2MoO_4 + 0.200 M sorbitol (solid line), 0.100 M $FeCl_3$ + 0.200 M sorbitol (dashed-dotted line) or 0.070 M Na_2MoO_4 + 0.200 M sorbitol (dotted line) solutions; all solutions were at pH 11.40 adjusted with NaOH concentrated solution (Fig. 1(a)). In addition, these voltammograms can be seen in expanded scale in Fig. 1(b); this figure also presents the cathodic branches of the voltammograms for the iron-sorbitol complex solution (dashed-dotted line) and molybdate anions solution (dotted line) in the inset.

Fig. 2 shows the voltammetric curves of copper electrode obtained in the NaOH solution (at pH 11.40) in the presence (solid line) and absence (dashed-dotted line) of 0.200 M sorbitol. For the Cu substrate in the presence of sorbitol, the formation of a cathodic peak can be observed (cathodic peak potential, E_{pc}, of −0.73 V, cathodic peak charge density, q_{pc}, of 9.30 mCcm^{-2}); this peak can be attributed to the reduction of copper oxide (formed with exposure to air after polishing the copper electrode). In addition, beyond −1.20 V, the current density, j, quickly increased due to the hydrogen evolution reaction (HER) (see inset in Fig. 2, solid line). The cathodic voltammogram in the absence of sorbitol (Fig. 2, dashed-dotted line) shows the formation of a cathodic peak (E_{pc}-0.75 V, q_{pc}7.8 mCcm^{-2}) due to the reduction of copper oxide (see also inset in Fig. 2, dashed-dotted line). Fig. 2 also shows that HER is more significant in the presence of sorbitol, i.e., at ~ -1.40 V j was ~-1.12 mAcm^{-2} and ~-0.42 mAcm^{-2}, respectively with and without sorbitol.

The anodic branch for the Cu electrode in the presence of sorbitol (solid line) shows the formation of an anodic region from ~-0.57 V to ~+0.40 V, anodic charge density (q_a) ~8.70 mCcm^{-2}. In the absence of sorbitol (dashed-dotted line) an anodic region from ~-0.50 V to ~+0.40 V, q_a ~4.90 mCcm^{-2} was observed (see inset graph of Fig. 2). Comparing the anodic branches in Fig. 2, it can be

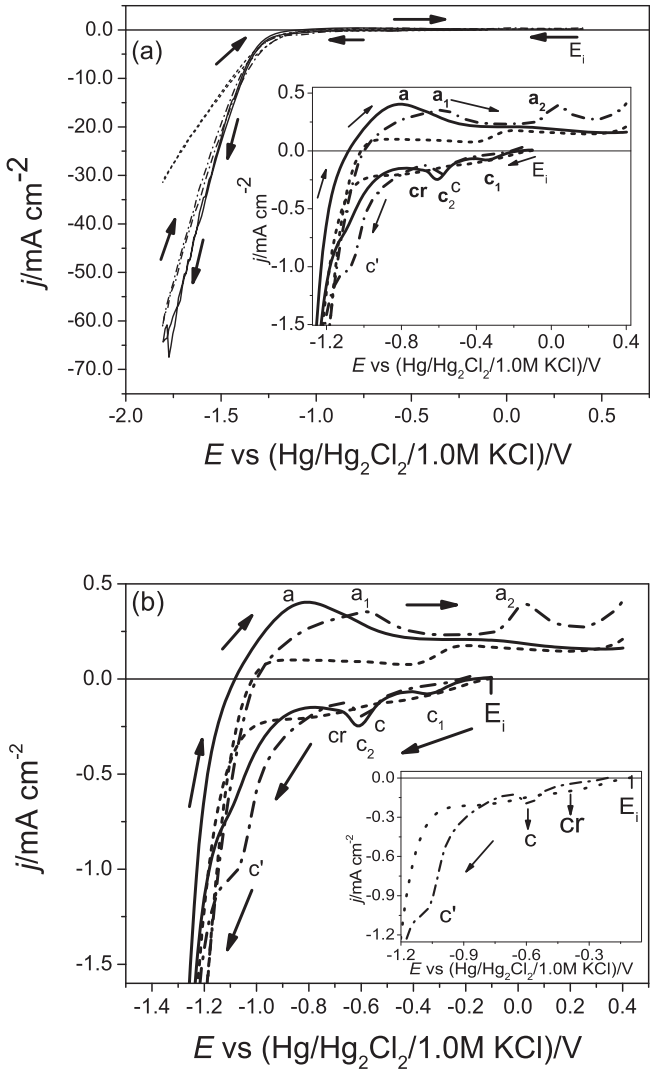

Fig. 1. (a). Voltammetric curves for Cu substrate in: 0.100 M $FeCl_3$ + 0.070 M Na_2MoO_4 (solid line); 0.100 M $FeCl_3$ (dashed–dotted line) or 0.070 M Na_2MoO_4 (dotted line). All solutions containing 0.200 M sorbitol and pH were adjusted at 11.40 with conc. NaOH. (b): voltammetric curves of the (a) with expanded axes and inset of cathodic branches of Fe(III)-sorbitol complex and $[MoO_4]^{2-}$ anions solutions voltammograms. v = 10.0 mVs^{-1}.

inferred that the dissolution of copper was facilitated in the presence of sorbitol, since its dissolution begins at a more negative potential (~-0.57 V) than it is observed in the absence of sorbitol (~-0.50 V). Literature [7] informs that, copper ions can be complexed by sorbitol. Thus, the fact that dissolution of copper in the presence of sorbitol occurred at potential more negative than in its absence can be explained by sorbitol adsorption and copper complexation.

The Fe-Mo deposition voltammogram (Fig. 1 (b), solid line) was characterized by two cathodic peaks c_1 (peak potential (E_p) ~-0.33 V) and c_2 (E_p ~ -0.61 V) and also by a steep increasing in the j at ~ -1.00 V due to the HER in parallel with Fe-Mo deposition (see Table 1).

Analyzing the Fe deposition curve (Fig. 1 (b), dashed-dotted line), the formation of a cathodic peak c (E_p ~ -0.59 V, $q_p = 3.68\ mCcm^{-2}$) and a wave c' (~-1.06 V) can be noted; this can be observed more clearly in the inset graph of this Fig. The current density increased significantly from ~-1.15 V due to the reduction of Fe^{3+} ions (as can be seen further) concomitant with the HER.

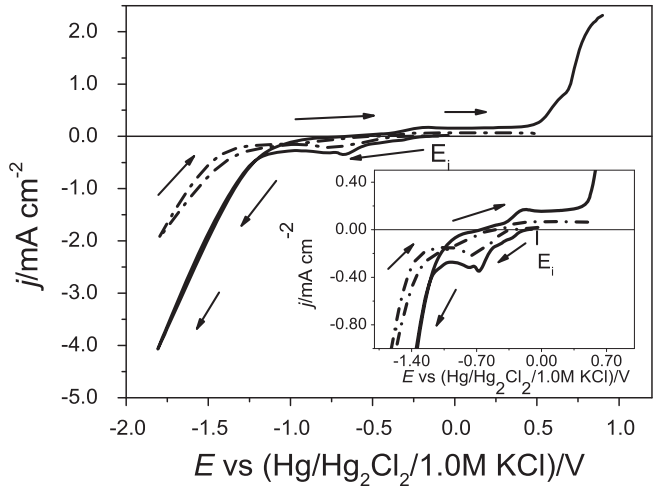

Fig. 2. Cyclic voltammetry for Cu substrate in 0.200 M sorbitol (solid line) and NaOH (dashed–dotted line) solutions, both at pH 11.40; inset in this Fig. with expanded axes. v = 10.0 mVs^{-1}.

Table 1
Chemical composition of the Fe-Mo films voltammetrically electrodeposited at various final deposition potentials (E_f), from 0.100 M $FeCl_3$ + 0.070 M Na_2MoO_4 + 0.200 M sorbitol bath at pH 11.40.

E_f/V	O(at%)	Fe(at%)	Mo(at%)
−0.33	88.6	8.45	2.9
−0.40	90.6	6.2	3.2
−0.68	86.1	10.8	3.2
−0.90	93.0	4.9	2.1
−1.80	86.8	9.1	4.1

EDXS analysis of the electrodeposits produced voltammetrically from the 0.100 M $FeCl_3$ + 0.070 M Na_2MoO_4 + 0.200 M sorbitol bath, at pH 11.40, for final electrodeposition potentials (E_f) of −0.33 V, −0.40 V, −0.68 V, −0.90 V and −1.80 V, then the sweep was reversed and the electrodeposition continued until the current density returned to zero, i.e., before moving to the anodic branch.

It can be noted in Table 1 that electrodeposits contained Fe, Mo and O, regardless of E_f.

The oxygen contents in Table 1 show that the Fe-Mo deposits could contain oxides/hydroxides of iron and/or molybdenum, presumably formed with exposure to air and also during electrodeposition process [5].

Fig. 1(b) shows the voltammetric curve for the Cu substrate in 0.070 M Na_2MoO_4 + 0.200 M sorbitol solution at pH 11.40 (dotted line). The formation of a cathodic region (cr) from ~-0.10 V to ~ -1.00 V (j_{cr} was ~-0.164 $mAcm^{-2}$) can be noted in this Fig.; in addition, beyond ~ -1.00 V j quickly increased due to the reduction of the molybdate anion to oxide/hydroxide [2–5,18] in parallel to the HER (see also the inset graph in this Fig., dotted line).

EDXS analysis of the films produced voltammetrically from the solution reported previously, for E_f values of −1.00 V and −1.80 V was performed. Also, after reaching each potential final, the voltammetric deposition continued until current density achieved value zero. The EDXS results showed that the film produced at E_f −1.00 V contained 2.8 at% (14.9 wt%) Mo and 97.2 at% (85.1 wt%) O and that the film produced at −1.80 V contained 3.6 at% (18.4 wt %) Mo and 96.4 at% (81.6 wt%) O. Therefore, these results indicate the transformation of $[MoO_4]^{2-}$ into the molybdenum oxide/hydroxide.

XRD analysis of the film produced voltammetrically from 0.070 M Na_2MoO_4 + 0.200 M sorbitol solution at pH 11.40 in the

potential range from −0.10 V to −1.10 V, holding the potential at −1.10 V for 2 h, was performed (Fig. 3). Moreover, after this time the electrodeposition continued until j returned to zero, i.e., before moving to the anodic branch.

A broad peak between 2θ ~12.5° and ~40° can be seen in the diffractogram of this film (Fig. 3). Thus, the crystallographic distances, d(h k l), were calculated considering the 2θ contained in the region of the broad peak. The crystallographic distances observed, d_{obs}(h k l), were compared with expected crystallographic distances, d_{exp}(h k l), for molybdenum oxide supplied by the JCPDS [19] and the result obtained, from this comparison, indicates the presence of the MoO_2 amorphous phase (JCPDS - 05–0452) in this electrodeposited film.

Reductive electrolysis of the Fe(III)-sorbitol complex was performed in the regions of the cathodic peak c (E_p ~ -0.59 V) and cathodic wave c' (~-1.06 V) and at q = 5C, from 0.100 M $FeCl_3$ + 0.200 M sorbitol solution (pH 11.40).

To verify the formation of the Fe(II) intermediate species, 1,10-phenanthroline (0.25%) was added to the solution immediately after completion of the electrolysis. It was noted that the yellow solution turned into a red solution only when the electrolysis was produced at −1.06 V (wave c'). This solution was analyzed by Visible spectroscopy and the absorption spectrum displayed a broad and intense absorption with maximum at 514 nm (Fig. 4, solid line), which is characteristic of the $[Fe(phen)_3]^{2+}$complex [20].

Similar electrolysis experiments were performed with a 0.100 M $FeCl_3$ + 0.070 M Na_2MoO_4+ 0.200 M sorbitol solution (pH 11.40) at −0.33 V (Ep_{c1}, Fig. 1). In agreement with the results presented above, the absorption spectrum of the solution displayed the maximum at 514 nm (Fig. 4, dashed line). Therefore, the formation of $[Fe(OH)_2(C_6H_{12}O_6)_2]^{4-}$ by reduction of $[Fe(OH)_2(C_6H_{12}O_6)_2]^{3-}$ on the metal/solution interface before the deposition of the alloy was detected by Visible spectroscopy.

Taking into account these findings, the cathodic processes on the Fe-Mo curve (Fig. 1(b), solid line) were due to reduction of $[Fe(OH)_2(C_6H_{12}O_6)_2]^{3-}$ to $[Fe(OH)_2(C_6H_{12}O_6)_2]^{4-}$ concomitant with the reduction of $[MoO_4]^{2-}$ to molybdenum(IV) oxide/hydroxide (peak c_1, see Figs. 1(b) and Fig. 3) and reduction of $[Fe(OH)_2(C_6H_{12}O_6)_2]^{4-}$ to Fe^0 concomitant with the reduction of molybdenum(IV) oxide/hydroxide to Mo^0 in parallel to the HER (peak c_2, see Fig. 1(b)).

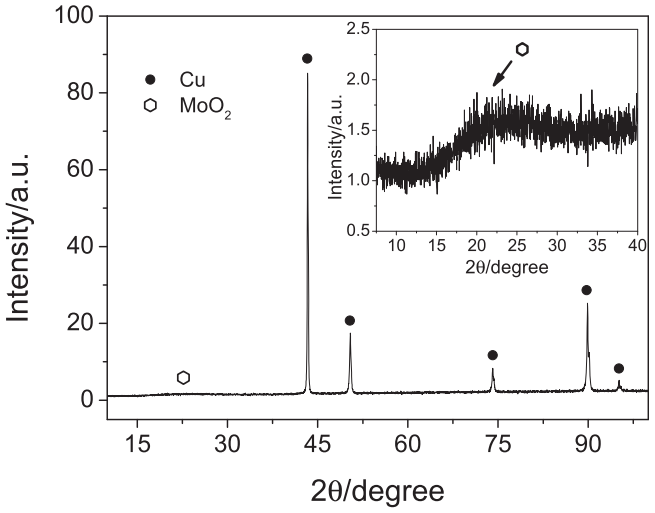

Fig. 3. Diffractogram of film produced voltammetrically, from 0.070 M Na_2MoO_4 + 0.200 M sorbitol solution at pH 11.40, in the potential range from −0.10 V to −1.10 V, with hold potential at −1.10 V for 2 h MoO_2 (JCPDS −05-0452), Cu (JCPDS - 04–0802).

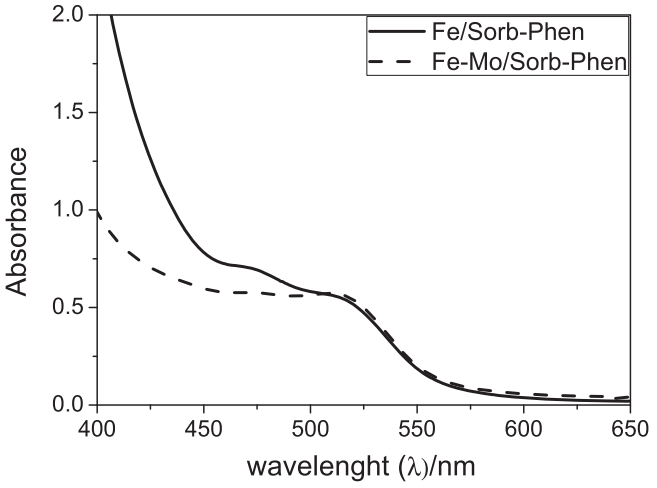

Fig. 4. Visible spectra of the final solution produced after electrolysis of the 0.100 M $FeCl_3$ + 0.200 M sorbitol solution (pH 11.40) (–) at −1.06 V and 0.100 M $FeCl_3$ + 0.070 M Na_2MoO_4+ 0.200 M sorbitol solution (pH 11.40) at −0.33 V(- - -), which were added 0.25% M 1,10-phenanthroline in the solution immediately after completion of electrolysis.

For the Fe voltammetric deposition curve (see inset in Fig. 1 (b), dashed-dotted line), the cathodic peak c (E_p ~ -0.59 V, $q_p = 3.68\ mCcm^{-2}$) can be associated to the adsorption of Fe(III) complex species and wave c' (~-1.06 V) to the reduction of $[Fe(OH)_2(C_6H_{12}O_6)_2]^{3-}$ to form $[Fe(OH)_2(C_6H_{12}O_6)_2]^{4-}$. In addition, after wave c', $[Fe(OH)_2(C_6H_{12}O_6)_2]^{4-}$ is reduced to Fe^0 with the concomitant HER.

It must be remembered that, peak c_1 (E_p ~ -0.33 V) from the Fe-Mo voltammetric curve (solid line, Fig. 1(b)) was meaningly depolarized with respect to wave c' (~-1.06 V) from the Fe voltammetric curve (dashed-dotted line). This fact can be explained by the adsorption of molybdate anions [5,21] on the copper electrode.

Fe-Mo anodic voltammetric curve (Fig. 1(b), solid line), showed a broad anodic region from ~-1.08 V to ~ -0.40 V. For potentials more positive than ~ -0.40 V, dissolution/passivation of the copper substrate occurred (see Fig. 2, solid line) [18].

It can be verified in the Fe anodic voltammetric curve (Fig. 1(b), dashed-dotted line) the formation of an anodic region a_1 (from ~-1.00 V to ~ -0.40 V) and an anodic peak a_2 (E_p~+0.020 V, due to the dissolution/passivation of Cu, see Fig. 2, solid line) [18]. Also, in both cases, it was observed that the deposit did not dissolve completely, since the film was visible to the naked eye after the end of the anodic scan (Fig. 1(b)).

The anodic processes a_1 and a_2 (in the Fe voltammetric curve, dashed-dotted line, Fig. 1(b)) were shifted to more positive potentials than that of the anodic process a (in the Fe-Mo voltammetric curve, solid line, Fig. 1(b)). Thus, these results indicate that Fe-Mo dissolution was not hindered by $[MoO_4]^{2-}$ anions. Already, in the case reported in the literature [5] the electrodeposits produced voltammetrically in the same potential region of present work were formed of iron and, the dissolution of these electrodeposits was polarized in the presence of molybdate anions.

The anodic voltammetric curve for the copper substrate in a $[MoO_4]^{2-}$ solution at pH 11.40 (Fig. 1(b), dotted line) showed anodic regions from ~-1.00 V to ~ -0.39 V and from ~-0.39 V to ~+0.40 V, which correspond, respectively, to the transformation of molybdenum (IV) oxide/hydroxide into $[MoO_4]^{2-}$ [18] and to the dissolution/passivation of copper (see inset graph in Fig. 2, solid line).

Table 2 shows the anodic/cathodic charge density ratio (q_a/q_c) for Fe-Mo voltammetric electrodeposition at several final electrodeposition potentials (E_f). It can be noted in Table 2 that the q_a/q_c

Table 2
Effect of cathodic limit potential (E_f) on the cathodic (q_c) and anodic (q_a) charge densities and the q_a/q_c ratio of Fe-Mo deposits from 0.100 M $FeCl_3$ + 0.070 M Na_2MoO_4 + 0.200 M sorbitol bath at pH 11.40 on a copper substrate.

E_f/V	q_a/q_c(%)
−0.40	245.48
−0.60	187.35
−1.00	83.01
−1.10	44.34
−1.20	24.42
−1.40	7.72
−1.60	1.44
−1.80	0.67

ratios were lower 100% due to: (1) HER (see Fig. 2) in parallel to Fe-Mo electrodeposition, (2) Fe passivation, which occur at pH ~11 [18]; the Mo (from the Fe-Mo film) dissolved as $[MoO_4]^{2-}$ [18]. These processes affected negatively the q_a/q_c ratios. The q_a/q_c ratios at E_f −0.40 V and −0.60 V exceeded 100%. This occurred since these Fe-Mo coatings possibly did not cover the copper substrate totally. Thus, in these regions, without electrodeposits, Cu passivation occurred. Pourbaix [18] reports that the copper dissolution/passivation can occur at pH ~11.

Voltammetric electrodeposition of Fe-Mo onto copper electrode, in 0.100 M $FeCl_3$ + 0.070 M Na_2MoO_4 + 0.200 M sorbitol bath (pH 11.40), was performed at different sweep rates and at various rotation speeds to study deposition process, as following.

Fig. 5(a) shows that current densities of the peaks c_1 (j_{pc1}) and c_2 (j_{pc2}) rose with increasing sweep rates (v). Fig. 5(b) shows that the j_{pc1} and j_{pc2} did not increase linearly with $v^{1/2}$ [22,23].

Therefore, these results suggest that, the reduction processes of the Fe-sorbitol complex and molybdate anions in the regions of peaks c_1 and c_2 were quasi reversible [24].

Also, the Fe-Mo electrodeposition voltammetric curves with the copper rotating disc electrode at various rotation speeds (w) were carried out in 0.100 M $FeCl_3$ + 0.070 M Na_2MoO_4 + 0.200 M sorbitol bath at pH 11.40. These experiments were performed to investigate the influence of the rotation speed of the copper disk electrode on the reduction current density of the species present in the deposition bath.

Literature [24] report that for an irreversible reaction, the deposition current density (j) was described for equation (1):

$$\frac{1}{j} = \frac{1}{j_k} + \frac{1}{j_{l,c}} \quad (1)$$

Fig. 6 shows plot of j^{-1} versus $w^{-1/2}$, where w is angular velocity, for −0.85 V (region of peak c_2, Fig. 1), which was linear.

It must be stressed that in the region of peak c_2 there are three cathode reactions occurring, as reported previously. The results obtained herein showed that the reduction current density increased with w. However, it is difficult to indicate, from these results, which reduction reaction was controlled by mass transport.

3.3. Characterization of the Fe-Mo electrodeposits produced potentiostatically

3.3.1. SEM

Fe-Mo electrodeposits produced at E_d values of −1.00 V, −1.20 V, −1.40 V, −1.60 V and −1.80 V from a sorbitol alkaline bath with q_d 5.30Ccm^{-2} were analyzed by SEM to verify the influence of various E_d on their morphologies (Fig. 7(a)-(e)). The photomicrography of the electrodeposits obtained at E_d −1.00 V

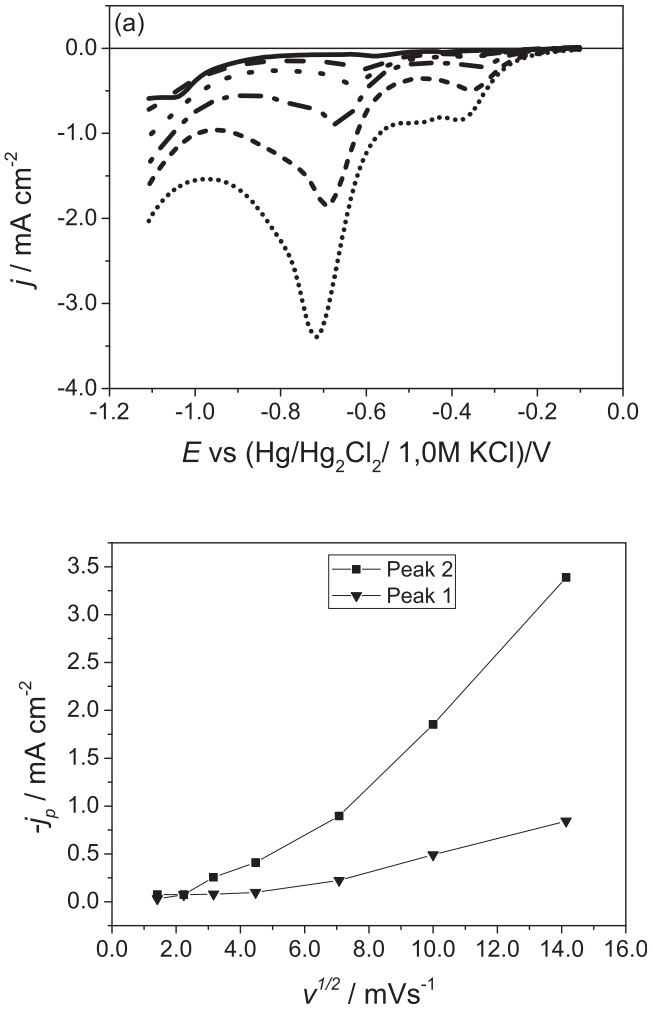

Fig. 5. Voltammetric curves for Cu substrates in 0.100 M $FeCl_3$ + 0.070 M Na_2MoO_4+ 0.200 M sorbitol at pH 11.40 with NaOH. (a) at various sweep rates (v/mV s^{-1}): (−) 2.0; (- - -) 10.0; (...) 20.0; (-·-·-) 50.0; (- - -) 100.0; (...) 200.0; (b) variation of j_{pc1} and j_{pc2} with $v^{1/2}$.

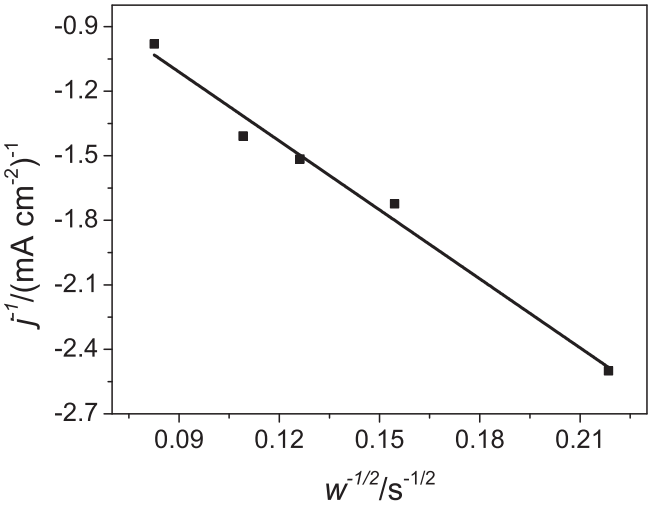

Fig. 6. Plot of j^{-1} versus $w^{-1/2}$ obtained from voltammetric curves for a rotating copper substrate in 0.100 M $FeCl_3$ + 0.070 M Na_2MoO_4+ 0.200 M sorbitol at pH 11.40 with NaOH υ = 2.0 mV s^{-1}.

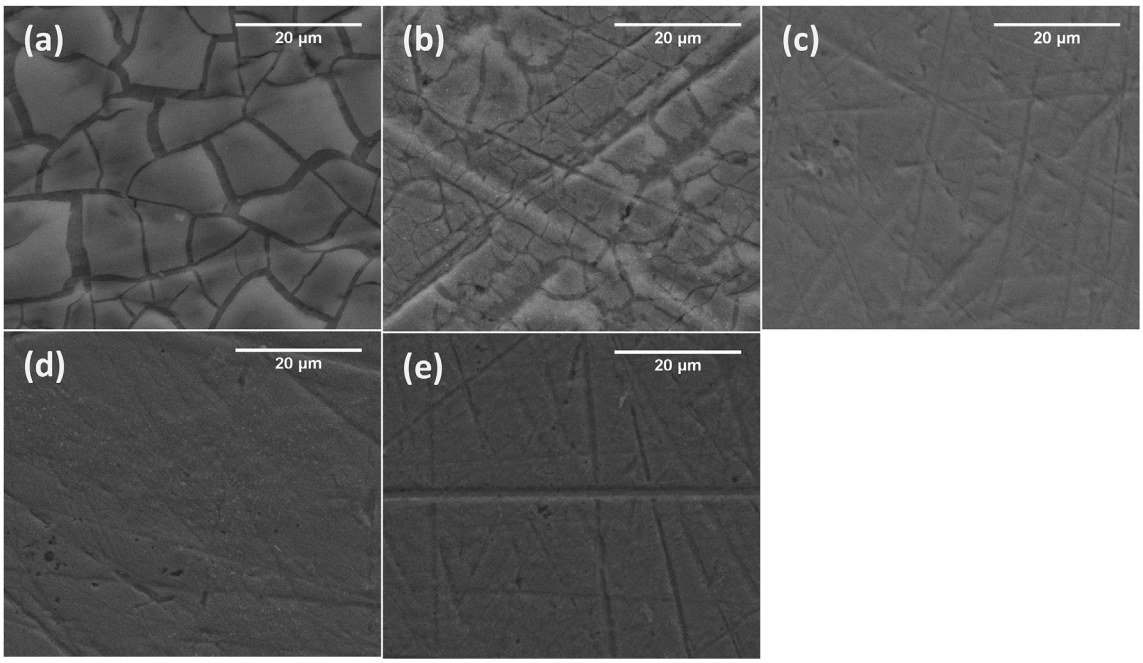

Fig. 7. SEM micrographs of Fe-Mo electrodeposits obtained at E_d: (a) −1.00 V, (b) −1.20 V, (c) −1.40 V, (d) −1.60 V and (e) −1.80 V, with q_d 5.30Ccm^{-2}. Electrolytic solution: 0.100 M $FeCl_3$ + 0.070 M Na_2MoO_4+ 0.200 M sorbitol at pH 11.40 with NaOH.

and −1.20 V presented in Fig. 7(a) and (b), respectively, showed a deposit covering the substrate, which exhibited cracks. However, the micrographs of the electrodeposits produced at E_d values of −1.40 V (Fig. 7(c)), −1.60 V (Fig. 7(d)) and −1.80 V (Fig. 7(e)), showed a thin film covering the substrate. The low thickness of these coatings is shown by the lines of the polishing substrate, which can be seen in these micrographs. Authors [5] found that of Fe-Mo electrodeposits produced with 0.055 M NTA in the deposition bath showed cracks, which can be associated to the presence of oxides in the electrodeposits, or globular clusters or crystallites coalesced crystallites globular depending E_d.

Kuznetsov et al. [25] investigated Fe-Mo electrodeposition from ammonia–citrate electrolyte and report that deposits presented cracks and microspheroids on the surface.

3.3.2. EDXS

EDXS analysis was performed to investigate the chemical composition of deposits produced as previously reported in section 3.3.1. It can be noted in Table 3 that Fe and Mo codeposition occurred and that the Mo content of the electrodeposits produced at E_d in the range from −1.00 V to −1.80 V varied from 1.2 at% to 5.5 at% or 4.9 wt% to 18.9 wt%.

The oxygen contents in Table 3 show that the Fe-Mo deposits could contain oxides/hydroxides of iron and/or molybdenum, presumably formed in the air and during electrodeposition process, as reported previously.

Table 3
Chemical composition of the Fe-Mo films potentiostatically electrodeposited from 0.100 M $FeCl_3$ + 0.070 M Na_2MoO_4 + 0.200 M sorbitol bath (pH 11.40), at various deposition potentials (E_d), with q_d 5.30Ccm^{-2}.

E_d/V	O(at%)	Fe(at%)	Mo(at%)	Ratio Fe/Mo
−1.00	79.5	18.9	1.7	11.1
−1.20	83.9	15.0	1.2	12.5
−1.40	74.9	19.6	5.5	3.6
−1.60	86.9	8.7	4.4	2.0
−1.80	88.1	7.5	4.4	1.7

As reported previously, electrodeposits produced at −1.00 V (Fig. 7(a)) and −1.20 V (Fig. 7(b)) showed cracks. However, those produced at −1.60 V (Fig. 7(d)) and −1.80 V (Fig. 7(e)) did not show cracks possibly due to being too thin.

Several authors have investigated the Fe-Mo electrodeposition and have reported that the Mo content in the electrodeposits was in the range from ~20 wt% to ~75 wt% [2–6,25–29].

The Mo content in the electrodeposits produced, from this study, (1.2 at% to 5.5 at% or 4.9 wt% to 18.9 wt% Mo) were lower than those related in the literature [2–6,24–28]. These results showed that Fe^{3+} and $[MoO_4]^{2-}$ salts concentration, complexing agent, pH, potentiostatic or galvanostatic electrodeposition [2–6,25–27,29], methods not electrochemical [28] affected the chemical composition of electrodeposits.

3.3.3. XRD

Structural phases of the Fe-Mo deposits, produced as previously reported in section 3.3.1, was investigated by X-ray diffraction analysis (Fig. 8(a)–(e)).

Fig. 8(a)-(e) show diffractograms of Fe-Mo electrodeposits, which present peaks around $2\theta = 39.1°$, 41.6°, 43.4°, 48.3°, 50.6°, 90.1°, 95.1° and 116.9°. The calculation of the crystallographic observed distances (d_{hkl}) from these angles and comparison with the expected values given in JCPDS cards [19] were performed.

The results indicate the presence of Fe_3Mo phase for $2\theta = 39.1°$ and 48.3° and, Fe_3Mo and Fe_2MoO_4 phases for $2\theta = 41.6°$ [19]. Also, some peaks ($2\theta = 90.1°$) could be attributed to Cu, Fe_3Mo and Fe_2MoO_4 phases and others ($2\theta = 43.4°$, 50.6° and 95.1°) to Cu and Fe_3Mo phases and to Cu phase ($2\theta = 116.9°$) (see Fig. 8(a)-(e)).

Reference [30] reported that the number of phases seems to be related with the surface morphology of the deposit. This was not the case of the present work, since the Fe-Mo morphologies were not always similar.

In addition, it can be noted from Fig. 8 that the diffractograms were indicative of a material with low crystallinity, because the peaks are broad [31].

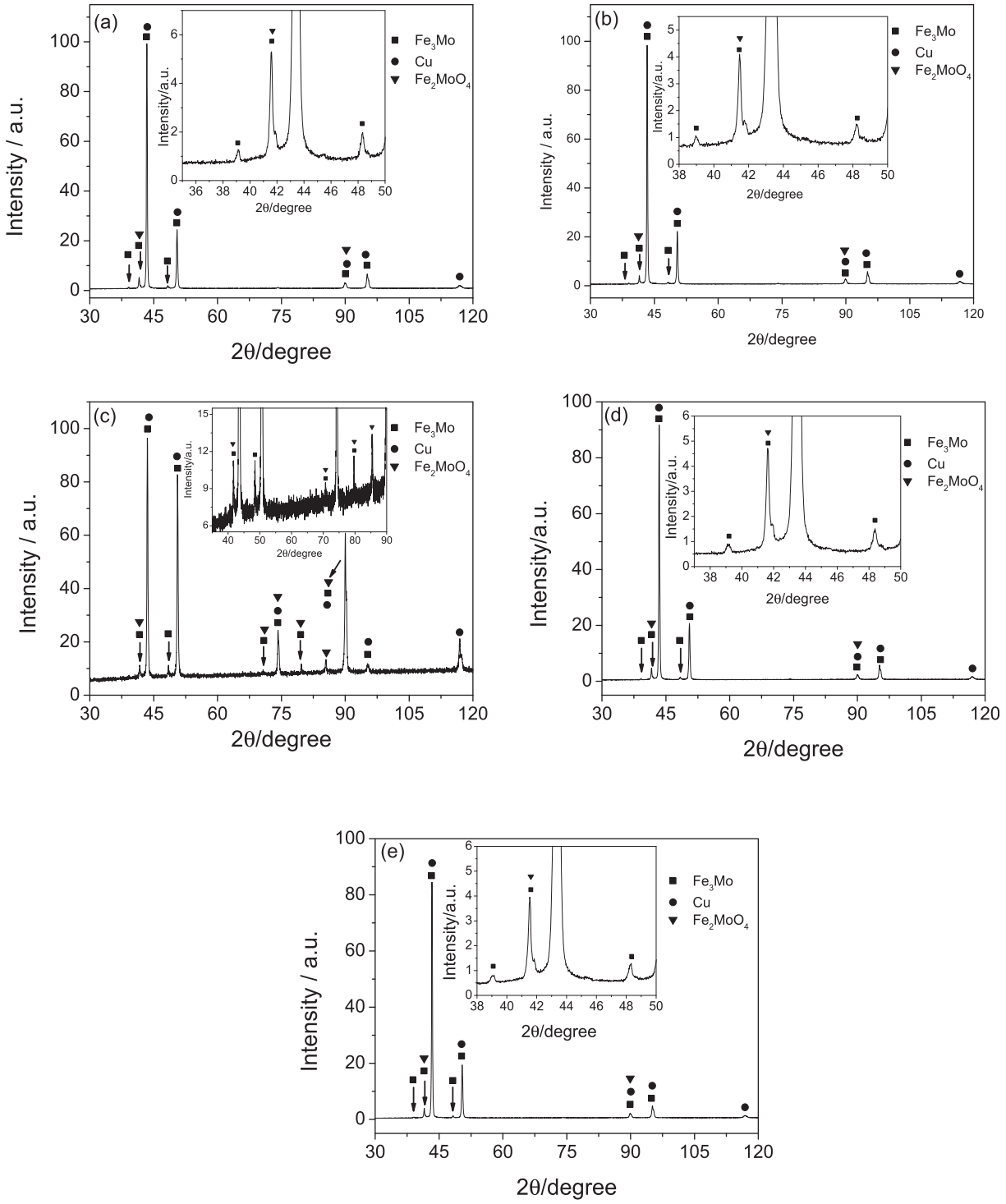

Fig. 8. Diffractograms of electrodeposits obtained at E_d: (a) −1.00 V, (b) −1.20 V, (c) −1.40 V, (d) −1.60 V and (e) −1.80 V, with q_d 5.30Ccm^{-2}. Electrolytic solution: 0.100 M $FeCl_3$ + 0.070 M Na_2MoO_4+ 0.200 M sorbitol at pH 11.40 with NaOH. Fe_3Mo (JCPDS - 31–0641), Cu (JCPDS - 04–0802) and Fe_2MoO_4 (JCPDS - 73236).

Kuznetsov et al. [27] investigated Fe-Mo alloys from ammonium-citrate baths and verified that electrodeposits with ~30 at% of molybdenum content were amorphous. As reported previously, the Mo content of the electrodeposits produced herein varied from 1.2 at% to 5.5 at%; these electrodeposits, considering the XRD results, were not amorphous but showed low crystallinity.

Opposing the results produced herein, the XRD analysis of Fe-Mo electrodeposits produced from a NTA alkaline bath [5] indicated that Fe_3Mo electrodeposits of very low crystallinity or partially amorphous were produced on Pt substrates.

The crystal sizes (t) [31] of the alloy can be calculated using the Debye-Scherrer formula as given below:

$$t = \frac{0.94\,\lambda}{B\cos\theta} \tag{2}$$

where t = crystal size (in nm), 0.94 is the Scherrer constant, λ is the wavelength of the radiation used ($\lambda_{Cu\text{-}K\alpha} = 0.154$ nm), B is the full width at half maximum (in radian), and Θ is the position of the maximum of the diffraction angle.

The peak corresponding to Fe_3Mo and Fe_2MoO_4 ($2\theta = 41.6°$) phases was used to calculate the crystal size (t). The estimated crystal size present in the Fe-Mo coatings varied in the range from 47 nm to 37 nm when E_d changed to more negative values.

The decreases in the Fe-Mo crystal size were associated to the more negative deposition potential, since nucleation and smaller crystallite sizes were favored [32].

Novakova et al. [28] investigated the formation of Fe–Mo compounds obtained by a not electrochemical method and verified that, for samples containing Mo in the range from 20 at% to 60 at%, the size of nanoparticles were in the range of ~10 nm–~30 nm.

3.3.4. XPS

The Fe 2p, O 1s, C 1s and Mo 3 d core-level electrons of Fe-Mo electrodeposits before and after sputtering process were investigated to study the chemical and electronic states of these species in the sample produced potentiostatically at −1.80 V with q_d 5.30Ccm^{-2} (Fig. 9). As expected, the amount of C element (Fig. 9(a)) decreased after 160 min of etching of Ar ions while the amount of O element (Fig. 9(b)) increased, indicating that a compound containing oxygen in the structure was present in the electrodeposit surface. The XPS spectrum of Fe 3p is shown in Fig. 9(c). As can be observed, after 30 min of etching, a significant modification is observed in both Fe3$p_{3/2}$ and Fe 3$p_{1/2}$ peaks. A similar trend was observed when de analysis of Mo 3 d high-resolution XPS spectra (Fig. 9(d)).

In order to interpret the changes in the high resolution XPS spectra of Fe and Mo before and after the etching process, CasaXPS software (Casa Software Ltd., UK) was used. Fig. 10 shows the high-resolution XPS spectra of Fe 2p and Mo 3 d elements before (0 min) and after 160 min of etching, which components were assigned according to the literature [33,34]. The Fe 2$p_{3/2}$ component before etching (0 min) can be resolved into two components that were assigned to Fe^{2+} (710.4 eV) and Fe^{3+} (711.9 eV) states [33]. The Mo 3$d_{5/2}$ (232.1 eV) and Mo 3$d_{3/2}$ (235.3 eV) components before etching (0 min) were assigned according to the literature to the Mo^{6+} state [34]. The binding energies of Fe 2$p_{3/2}$ and Fe 2$p_{1/2}$ after 160 min are 709.4 eV and 724 eV, respectively. The satellite peak for Fe 2$p_{3/2}$ was observed at 712.7 eV. The presence of this "shoulder" satellite peak and the binding energies of Fe 2$p_{3/2}$ and Fe 2$p_{1/2}$ components indicates the presence of only Fe^{2+} states [33,35].

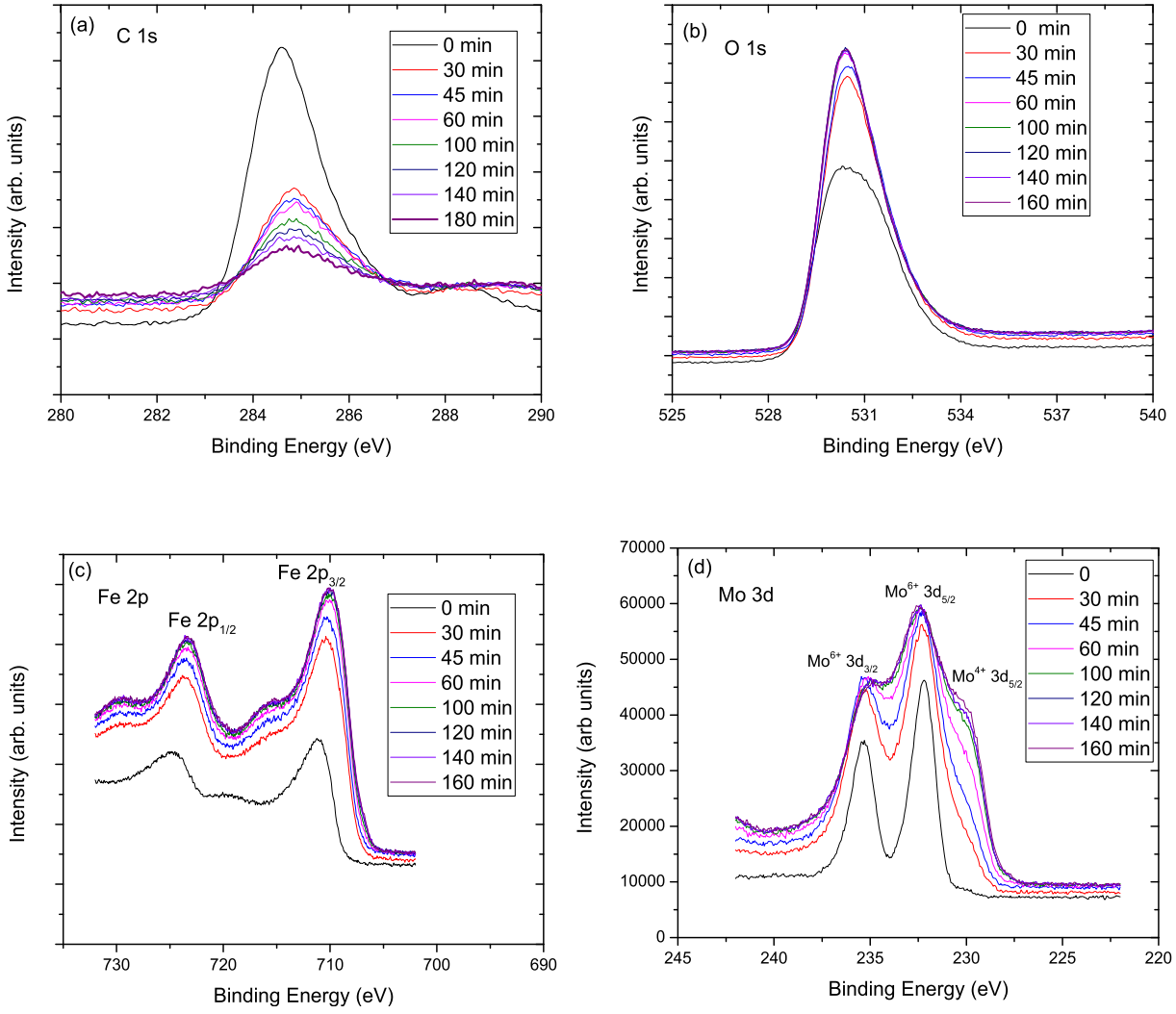

Fig. 9. –High-resolution XPS spectra of the Fe-Mo electrodeposit produced at −1.80 V, with q_d 5.30Ccm^{-2}, as a function of the etching time: (a) C1s, (b) O 1s, (c) Fe 2p and (d) Mo 3 d states. Electrolytic solution: 0.100 M $FeCl_3$ + 0.070 M Na_2MoO_4+ 0.200 M sorbitol at pH 11.40 with NaOH.

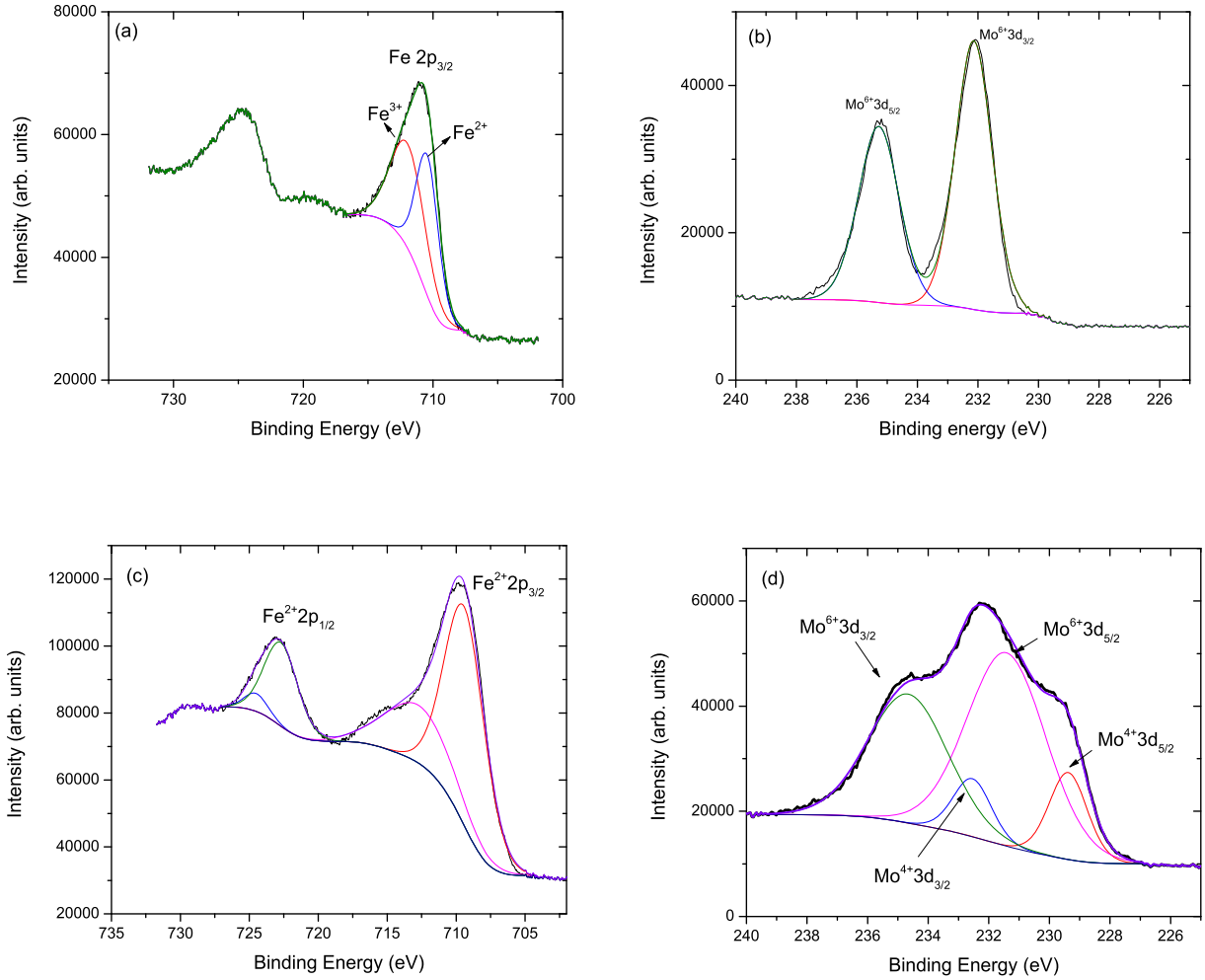

Fig. 10. High resolution of XPS spectra of Fe 2p and Mo 3 d states: (a) and (b) before etching and (c) and (d) after 160 min of etching of the Fe-Mo electrodeposit produced at −1.80 V, with q_d 5.30Ccm^{-2}. Electrolytic solution: 0.100 M $FeCl_3$ + 0.070 M Na_2MoO_4+ 0.200 M sorbitol at pH 11.40 with NaOH.

Concerning the high-resolution XPS spectrum of Mo 3 d after 160 min of etching, four components were observed by deconvolution. Besides the peaks of the Mo^{6+} state, two new peaks assigned to Mo^{4+} $3d_{5/2}$ (229.4 eV) and Mo^{4+} $3d_{3/2}$ (234.7 eV) appears and its intensity increases as the etching time increases, indicating the formation of Mo^{4+} species.

GIXRD analysis of the Fe-Mo electrodeposit after 160 min of etching was performed. It must be stressed that this electrodeposit was produced at −1.80 V with q_d 5.30Ccm^{-2}. According to the GIXRD experiment (Fig. 11), the presence of Fe_3Mo and Fe_2MoO_4 phases was observed on the sample surface. These results corroborated those obtained by conventional XRD experiments (Fig. 8).

The presence of Fe_2MoO_4 phase on the sample surface could explain the observation by XPS of Fe^{2+} and Mo^{4+} states. However, the observation of Fe^{3+} and Mo^{6+} indicates that others crystalline oxide phases, possibly such as, $FeMoO_4$ [36,37] and $Fe_2(MoO_4)_3$ [37] did not observed by XRD also exists on the sample surface.

Finally, it is worth mentioning that Fe_3Mo alloy [1,36], Fe_2MoO_4 [37], $FeMoO_4$ [36,37] and $Fe_2(MoO_4)_3$ [37] compounds are of great importance for the protection of corrosion. Thus, the results obtained in the present work led to infer that due to the presence of Fe_3Mo, Fe_2MoO_4 and, possibly $FeMoO_4$ and $Fe_2(MoO_4)_3$ phases, in the electrodeposits, these could be considered as a potential material against corrosion protection.

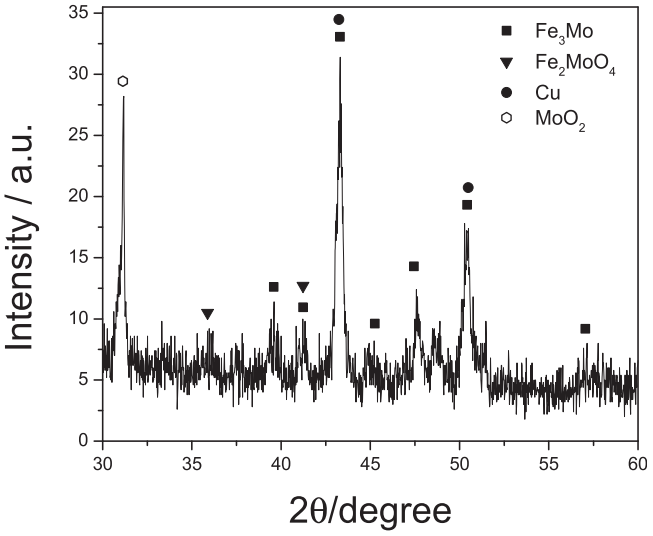

Fig. 11. Diffractograms of electrodeposits in grazing incidence mode, obtained at E_d: −1.80 V, with q_d 5.30Ccm^{-2}. Electrolytic solution: 0.100 M $FeCl_3$ + 0.070 M Na_2MoO_4+ 0.200 M sorbitol at pH 11.40 with NaOH. Fe_3Mo (JCPDS - 31–0641), Cu (JCPDS - 04–0802) and Fe_2MoO_4 (JCPDS - 73236).

4. Conclusions

1. The alkaline solution for Fe-Mo electrodeposition containing Fe(III)-sorbitol complex and molybdate anion, did not show precipitate as prepared at pH 11.40 and during the electrodeposition, indicating stability.
2. EDXS analysis of Fe-Mo electrodeposits produced in different regions of voltammetric curve showed that the deposited coatings were composed of Fe, Mo and O.
3. XRD analysis of the film produced voltammetrically by reduction of molybdate anions onto a copper substrate showed the formation of molybdenum oxide.
4. The presence of the intermediate Fe(II) species was detected by electrolysis from a Fe-Mo solution and Visible spectroscopy in the presence of 1,10-phenanthroline. The spectrum showed an absorption ($\lambda_{max} = 514$ nm) typical of the $[Fe(phen)_3]^{2+}$ complex.
5. Under our conditions, the Fe-Mo alloy was formed from reduction of $[Fe(OH)_2(C_6H_{12}O_6)_2]^{3-}$ to $[Fe(OH)_2(C_6H_{12}O_6)_2]^{4-}$, reduction of $[MoO_4]^{2-}$ to molybdenum (IV)oxide/hydroxide and its further reduction to Mo^0 concomitant with $[Fe(OH)_2(C_6H_{12}O_6)_2]^{4-}{}_{ads}$ to Fe^0.
6. With EDXS analysis was verified that the Mo content varied from 1.2 at% to 5.5 at% or 4.9 wt% to 18.9 wt%, depending on E_d.
7. The photomicrography of the electrodeposits showed cracks or a thin and uniform film, indicating that the nucleation and growth processes were not similar.
8. With X-Ray diffraction analysis, it was possible to conclude that the deposited coatings were formed of Fe_3Mo and Fe_2MoO_4 phases of low crystallinity, regardless of E_d.
9. From XPS analysis, it was possible to infer that the Fe, Mo and O elements in the electrodeposits were present in the sample surface which belongs, according XRD experiments, to the Fe_2MoO_4 phase and also to Fe and Mo oxides phases, possibly $FeMoO_4$ and $Fe_2(MoO_4)_3$.
10. The estimated crystal size value varied from ~47 nm to ~37 nm, when E_d changed to more negative values.

Thus, the results previously reported permitted to establish the steps for the electrodeposition of the Fe-Mo alloy, from the alkaline bath developed herein, which are important for controlling the conditions of production of such alloys.

Acknowledgements

The authors would like to acknowledge Fundação de Amparo à Pesquisa do Estado de São Paulo (FAPESP; Proc. 2008/57652-1) for the grants received.

References

[1] A. Brenner, Electrodeposition of Alloys: Principles and Practice, vol. 1, Academic Press, New York, 1963.
[2] D.W. Ernst, M.L. Holt, J. Electrochem. Soc. 105 (1958) 686–692.
[3] D. W. Ernst, R.F. Amlie, M.L. Holt, 105 (1955) 461–469.
[4] L.O. Case, A. Krohn, 105 (1958) 512–520.
[5] E.P. Barbano, M.F. de Carvalho, I.A. Carlos, J. Electroanal. Chem. 775 (2016) 146–156.
[6] H. Fukushima, T. Akiyama, S. Akagi, K. Higashi, Trans. Japan Inst. Metals 20 (1979) 358–364.
[7] L.L. Barbosa, M.R.H. de Almeida, R.M. Carlos, M. Yonashiro, G.M. Oliveira, I.A. Carlos, Surf. Coating. Technol. 192 (2005) 145–153.
[8] M.R.H. de Almeida, I.A. Carlos, L.L. Barbosa, R.M. Carlos, B.S. Lima-Neto, E.M.J.A. Pallone, J. Appl. Electrochem. 32 (2002) 763–773.
[9] E.M. de Oliveira, I.A. Carlos, Surf. Coating. Technol. 206 (2011) 250–256.
[10] E.M. de Oliveira, I.A. Carlos, J. Appl. Electrochem. 38 (2008) 1203–1210.
[11] M.S. Pereira, L.L. Barbosa, C.A.C. Souza, A.C.M. de Moraes, I.A. Carlos, J. Appl. Electrochem. 36 (2006) 727–732.
[12] E.M. Oliveira, G.A. Finazzi, I.A. Carlos, Surf. Coating. Technol. 200 (2006) 5978–5985.
[13] L.L. Barbosa, I.A. Carlos, Surf. Coating. Technol. 201 (2006) 1695–1703.
[14] M.R.H. de Almeida, E.P. Barbano, M.F. de Carvalho, P.C. Tulio, I.A. Carlos, Appl. Surf. Sci. 333 (2015) 13–22.
[15] J.L.P. Siqueira, I.A. Carlos, J. Power Sources 169 (2007) 361–368.
[16] G.A. Finazzi, E.M. de Oliveira, I.A. Carlos, Surf. Coating. Technol. 187 (2004) 377–387.
[17] M.G. Zacarin, Dissertation, University Federal of São Carlos (2016).
[18] M. Pourbaix, Atlas of Electrochemical Equilibria in Aqueous Solutions, second ed., Pergamon Press Ltd, Texas, USA, 1974.
[19] Joint Committee on Powder Diffraction Standards (JCPDS), in: International Centre for Diffraction Data. Powder Diffraction File PDF-2. Database Set 1–49, ICDD CD-ROM, Pennsylvania, 2000.
[20] P.S. Braterman, J.I. Song, R.D. Peacock, Inorg. Chem. 31 (1992) 555–559.
[21] U.S. Mohanty, B.C. Tripathy, P. Singh, S.C. Das, V.N. Misra, J. Appl. Electrochem. 38 (2008) 239–244.
[22] G. Mamantov, D.L. Manning, J.M. Dale, J. Electroanal. Chem. 9 (1965) 253–259.
[23] T. Berzins, P. Delahay, J. Am. Chem. Soc. 75 (1953) 555–559.
[24] J.A. Bard, L. Faulkner, Electrochemical Methods. Fundamentals and Applications, Wiley, New York, 1980.
[25] V.V. Kuznetsov, K.E. Golyanin, T.V. Pshenichkina, Elektrokhimiya 48 (2012) 1216–1221.
[26] N.R. Elezovic, B.N. Grgur, N.V. Krstajic, V.D. Jovic, J. Serb. Chem. Soc. 70 (2005) 879–889.
[27] V. Kuznetsov, K.E. Golyanin, Yu Sh Ladygina, T.V. Pshenichkina, B.F. Lyakhov, K.V. Pokholok, Russ. J. Electrochem. 51 (2015) 748–757.
[28] A.A. Novakova, T.Yu Kiseleva, V.V. Lyovina, D.V. Kuznetsov, A.L. Dzidziguri, J. Alloys Compd. 423 (2001) 317–427.
[29] M.V. Ved, N.D. Sakhnenko, A.V. Karakurchi, S.I. Zyubanova, Russ. J. Appl. Chem. 87 (2014) 276–282.
[30] R. Juskenas, Z. Mockus, S. Kanapeckaité, G. Stalnionis, A. Survila, Electrochim. Acta 52 (2006) 928–935.
[31] B.D. Cullity, S.R. Stock, Elements of X-ray Diffraction, Prentice-Hall, London (, 2001.
[32] E. Budevski, G. Staikov, W.J. Lorenz, Electrochim. Acta 45 (2000) 2559–2574.
[33] T. Yamashita, P. Hayes, Appl. Surf. Sci. 254 (2008) 2441–2449.
[34] M. Lv, W. Xie, S. Sun, G. Wu, L. Zheng, S. Chu, C. Chao, J. Bao, Catal. Sci. Technol 5 (2015) 2925–2934.
[35] K. Dey, A. Ghosh, P. Modak, A. Indra, S. Majumdar, S. Giri, Appl. Phys. Lett. 105 (2014), 142905.
[36] J.R. Ambrose, The role of molybdenum as an inhibitor of localized corrosion on iron in chloride solutions, Nat. Assoc. Corrosion Eng. 34 (1978) 27–31.
[37] N. Boucherit, A. Hugot-Le Goff, S. Joiret, Raman studies of corrosion films grown on Fe and Fe-6Mo in pitting conditions, Corrosion Sci. 32 (1991) 497–507.